Inverse-designed metasurfaces with facile fabrication parameters

IOP Publishing Journal of Optics
J. Opt. **26** (2024) 055101 (6pp) https://doi.org/10.1088/2040-8986/ad33a7

Inverse-designed metasurfaces with facile fabrication parameters

You Zhou[1,2,*], **Yixuan Shao**[1], **Chenkai Mao**[1] **and Jonathan A Fan**[1,*]

[1] Department of Electrical Engineering, Stanford University, Stanford, CA 94305, United States of America
[2] Department of Physics and Optical Science, University of North Carolina at Charlotte, Charlotte, NC 28223, United States of America

E-mail: zhouy7@stanford.edu, yzhou33@uncc.edu and jonfan@stanford.edu

Received 30 November 2023, revised 22 February 2024
Accepted for publication 13 March 2024
Published 21 March 2024

Abstract

Optical metasurfaces are planar nanostructured devices that are industrially attractive in part because they utilize high-throughput microelectronic fabrication techniques for implementation. It is therefore critical to develop design paradigms that can balance the realization of highly efficient wavefront responses together with device manufacturability. We introduce a gradient-based design framework for freeform metasurfaces in which nanoscale elements are explicitly constrained to feature basic shapes, nearly uniform feature sizes, and exceptionally low aspect ratios. In spite of the apparent uniformity of the metasurface geometric features, the devices are able to utilize nonlocal near-field optical coupling to achieve highly efficient and extreme wavefront scattering beyond conventional design methodologies. Utilizing this approach, we design facile high-numerical-aperture devices such as beam deflectors and large-area metalenses capable of diffraction-limited focusing. We anticipate that these concepts can facilitate the design and integration of metasurfaces into monolithic optical systems.

Supplementary material for this article is available online

Keywords: inverse-designed, metasurfaces, facile, fabrications, high numerical aperture

Optical metasurfaces have emerged as a versatile thin-film platform for manipulating the wavefront of light. Through proper engineering of subwavelength-scale features, metasurfaces have unlocked a wide range of applications, including lensing [1–4], holography [5, 6], polarimetry [7–11] and multifunctional elements [12–16]. Control of angular and spectral selectivity has also been achieved with nonlocal metasurfaces [17–19], which support tailored long-range interactions and have been utilized in image differentiation [19], wavefront selection [20], and biological imaging [21] applications. The tremendous growth of the metasurface field and its fast adoption in academia and industry is due in part to its compatibility with standard semiconductor manufacturing processes, which are mature and readily facilitate the patterning and monolithic integration of nanostructured thin-film systems. Metasurface designs that satisfy foundry design rules and feature fabrication-friendly shapes, element sizes, and aspect ratios are crucial for ensuring high manufacturing yield.

While much progress has been made in the domain of metasurface design, it remains a challenge to develop concepts that balance device performance with manufacturability. Conventional design methodologies [1, 22–24], which utilize libraries of simple, physically intuitive meta-atoms (figure 1(a)), offer a rapid design framework for creating large-area metasurfaces with low computational cost. However, it is challenging to achieve complex functionalities with these devices due to the limited design space and the meta-atoms typically feature high aspect ratios because they utilize dynamic phase accumulation to achieve a 2π phase response [24]. Freeform topology optimization design methods, including the adjoint variables method [25–27] and neural

* Authors to whom any correspondence should be addressed.

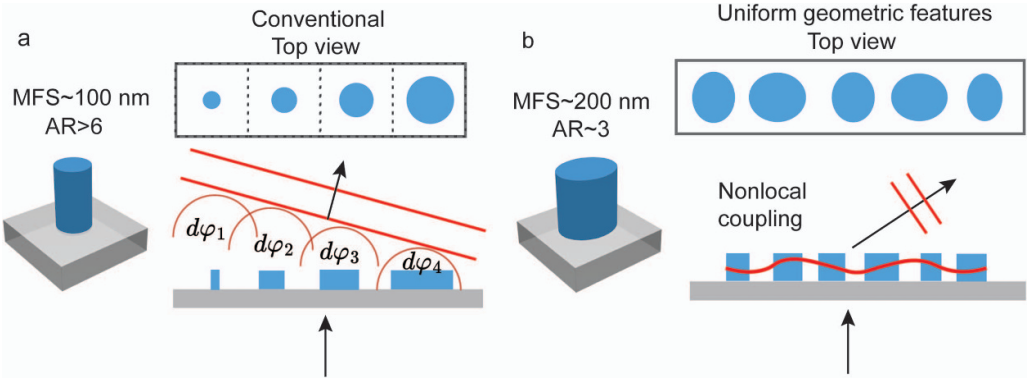

Figure 1. Conventional and reparameterized gradient-based design methods. (a) Schematic of conventional designs based on the local phase approximation. A library of discrete meta-atoms covering a 2π phase range results in structures with small minimum feature size (MFS) and high aspect ratio (AR). (b) Schematic of freeform devices designed using the proposed reparameterized gradient-based optimization algorithm. The meta-elements consist of simple elliptical nanoposts featuring large, nearly uniform sizes and low aspect ratios.

network-enabled algorithms [28], can significantly expand the nanophotonics design landscape to produce nanophotonic devices with new and enhanced capabilities [29–34]. However, these freeform devices are often challenging to fabricate due to their complex shapes [35], which can feature highly non-uniform material fill fractions, tight radii of curvatures [36–38], and high aspect ratios [32, 39] even after robustness criteria are incorporated in the design algorithms [35–38, 40–42].

In this study, we introduce a new freeform metasurface design regime that strikes a critical balance between performance and manufacturing. The concept, summarized in figure 1(b), shows meta-elements that are explicitly constrained to simply shaped, nearly uniformly sized, low-aspect-ratio nanostructures. As a freeform platform, near-field interactions between meta-elements are leveraged to enable tailored scattering responses beyond the limits of conventional phased array concepts (figure 1(b) bottom), in spite of the apparent geometric uniformity within the device. The use of relatively large elliptical shapes leads to facile lithographic patterning due to mitigation of local proximity error effects and the lack of tight radii of curvatures. The utilization of low-aspect-ratio elements relaxes the requirements and specifications of the etching process, leading to reduced variability in etch depths and sidewall profiles. Furthermore, the nearly uniformly sized, low-aspect-ratio features enable uniform material fill fractions, which enhance planarization compatibility crucial in multilayer lithography.

To streamline the enforcement of geometrical constraints within the gradient-based adjoint variables method, we utilize a reparameterization scheme that constrains freeform geometries to elliptically-shaped nanopost elements. The structural parameters of each element, including width, length, displacement, and rotation, are encoded as unbounded latent variables and are transformed to constrained geometric parameters using analytic mathematical transformations [43], shown in figure 2(a). Through this approach, the minimum feature sizes and gap sizes are rigorously enforced, and we specify these features to be relatively large to ensure that all elements are nearly uniformly sized. Since the transformation is fully analytic and differentiable, the scheme can be integrated with gradient-based optimization in which the gradients to the permittivity profiles are computed and readily backpropagated to update the latent variables using the chain rule (see details of the reparameterization formalism in supplementary).

These concepts can be used to design wavelength-scale 'super-pixels' capable of performing extreme scattering tasks, such as the selective scattering of normally incident light to large angles (figure 2(b)). As a proof-of-concept demonstration, we consider a 3λ-long, three-dimensional device that is surrounded by perfectly matched layers (PMLs) and is designed to scatter transverse magnetic polarized light to a 50° angle. The device is designed to operate at a wavelength of 900 nm and comprises a patterned 650 nm-thick silicon layer with a refractive index of 3.55 obtained by ellipsometry. The ellipses have minimal major and minor axes that are explicitly set to 190 nm. An example of a local gradient-based optimization trajectory from randomly initialized latent variables is depicted in figure 2(c) and shows the top view of permittivity profiles and the side view of electric field distributions for different iteration numbers. The device initially starts with randomized dielectric posts with grayscale permittivity values ranging between air and silicon. Over the course of optimization, the device evolves into an array of elliptical silicon nanoposts with gradually increasing deflection power towards the desired angle. The final device exhibits a minimal feature size of 190 nm, along with a maximum size variation of 170 nm and 28 nm along the x-direction and the y-direction, respectively. These values correspond to an average size variation of 49% and nanopost aspect ratios less than 3.4.

The performance of the final optimized device is validated by full-wave simulation using an open-source finite-difference time-domain solver, MIT electromagnetic equation propagation (MEEP) [44]. The final freeform device layout and its corresponding far-field scattering profile are presented in figure 3(a), showing strong directional scattering to the desired angle. To quantify the deflection performance, we

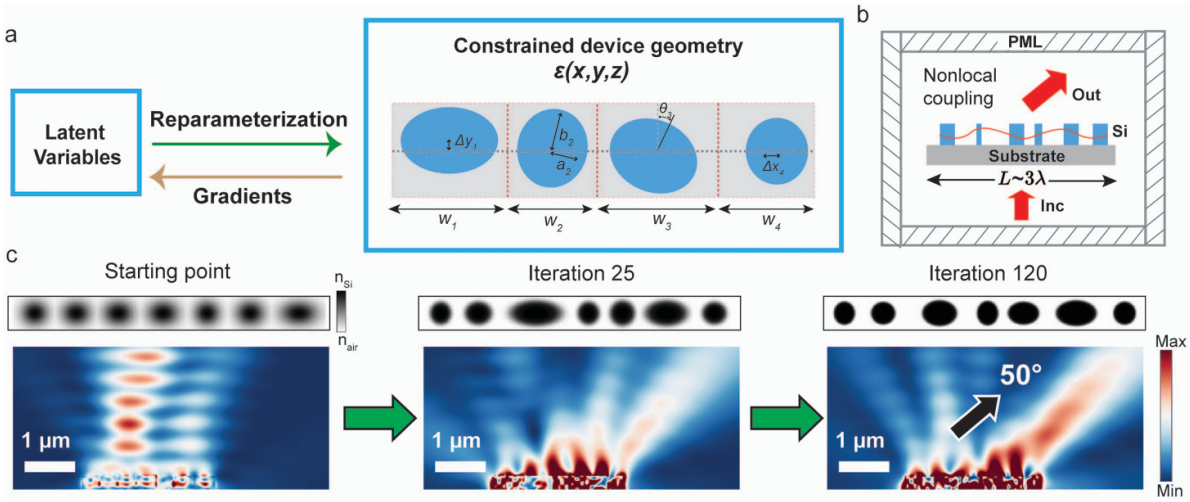

Figure 2. Reparameterization scheme for designing freeform aperiodic scatters. (a) Computational graph of the reparameterization process. Geometrical constraints are hard-coded into the device geometry via the analytic transformation of continuous latent variables to constrained device layouts. (b) A schematic of the optimization setting. The device, scaled at 3λ, is surrounded by perfectly matched layers (PMLs) and designed to scatter light to an arbitrary angle. (c) An example of the optimization trajectory of a 50° deflector. The top view of the permittivity profiles (top) and the side view of electric field distributions (bottom) are shown. The final device features a minimum nanopost size of 190 nm and an aspect ratio less than 3.4.

define relative and absolute efficiency as the ratios of power scattered in the desired direction to the transmitted power and to the total power, respectively. The final device achieves 80% relative efficiency and 64% absolute efficiency. As a point of comparison, we compare our reparametrized device with a conventionally designed device based on the local phase approximation (figures 3(c) and (d)). Figure 3(d) shows the resulting scatterer design and far-field scattering profile, which displays clearly visible parasitic side lobes. The relative and absolute deflection efficiencies are calculated to be 68% and 52%, respectively, which are approximately 20% lower than those of our freeform device.

The optimal scattering behavior in our freeform structure is attributed to the nonlocal coupling dynamics between adjacent nanostructures. The electric field distribution, shown in figure 3(a) (bottom), reveals strong nonlocal coupling between ellipses. The hybridized modes collectively break out-of-plane mirror symmetry and produce an effective surface impedance matching condition [45] that allows for highly efficient extreme scattering. We further investigate the impact of minimum nanopost feature size on the overall device performance. Figure 3(e) presents the absolute efficiencies and top view (inset) of the optimized 50° deflectors for minimum nanopost sizes ranging from 170 nm to 260 nm, showing that the absolute efficiencies remain above 55% for minimum sizes smaller than 220 nm.

Optimized super-pixel scatters can be utilized as building blocks to construct large-area freeform metasurfaces. A schematic of the design concept is shown in figure 4(a). The wavefront profile of the full-scale device is partitioned by a set of super-pixels [33], each of which scatters the incident light to a particular angle (θ) and phase (ϕ). In this manner, we approximate the desired phase profiles as a set of linear segments, which introduces a root-mean-square (RMS) wavefront error [33, 46] of:

$$\varepsilon_{\mathrm{rms}} = \frac{1}{12\sqrt{5}}\phi''(x_0)\,d^2.$$

With this expression, we find that linearizing phase profiles using 3λ-wide super-pixels introduces minimal wavefront error for most practical applications.

Our design strategy can enable the facile design of large-numerical-aperture metasurfaces. As a proof-of-concept demonstration, we consider a metalens that has a diameter of 81 μm and an NA of 0.7, thereby featuring super-pixels that scatter light up to a 44° angle. To account for the non-convex optimization landscape, we perform 30 optimizations with randomly generated latent variable initializations for each super-pixel and select the designs with the highest figure of merit, which balance efficiency and phase accuracy. Figure 4(b) presents the absolute efficiencies of the optimized super-pixels covering angles ranging from 23° to 44° and shows that the absolute efficiencies remain consistently high, above 70%, with minimal drop-off at larger angles. The inset shows the top views of super-pixels at three scattering angles, each enforced by the same geometrical constraints and each displaying arrays of nanoposts with near uniform dimensions. The full wave simulation of the full-scale metalens is in figure 4(c), and the axial intensity distribution plotted on a dB scale demonstrates efficient focusing with minimal spurious diffraction. The one-dimensional horizontal cut of

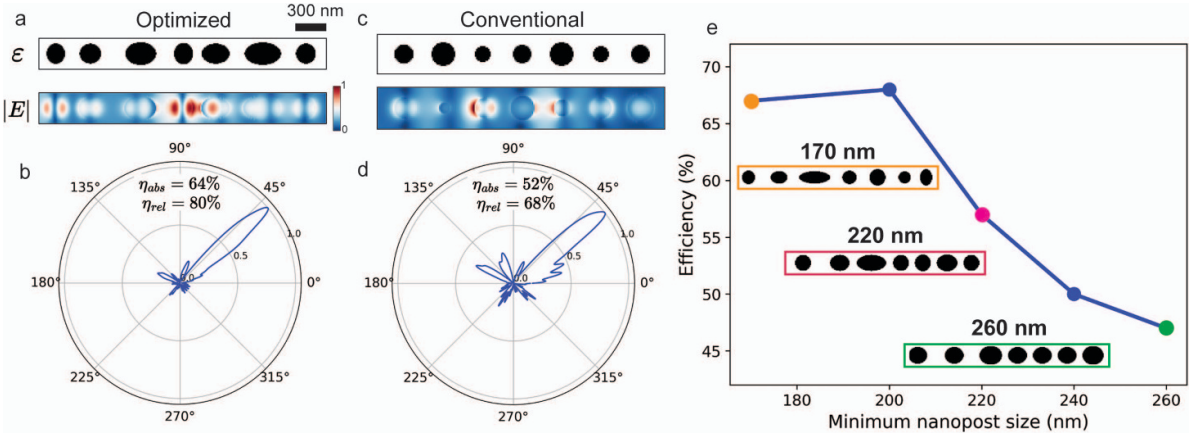

Figure 3. Comparison between reparameterized freeform scatters and conventional phase arrays. (a) Top view of the deflector (top) and electric field distribution (bottom) designed using reparameterization method. (b) Polar plot of far-field scattering. (c) Top view of deflector structures (top) and electric field distribution (bottom) designed using conventional method based on local phase approximation. (d) Polar plot of far-field scattering. (e) Absolute deflection efficiency of reparameterized freeform scatters for a range of minimum feature sizes.

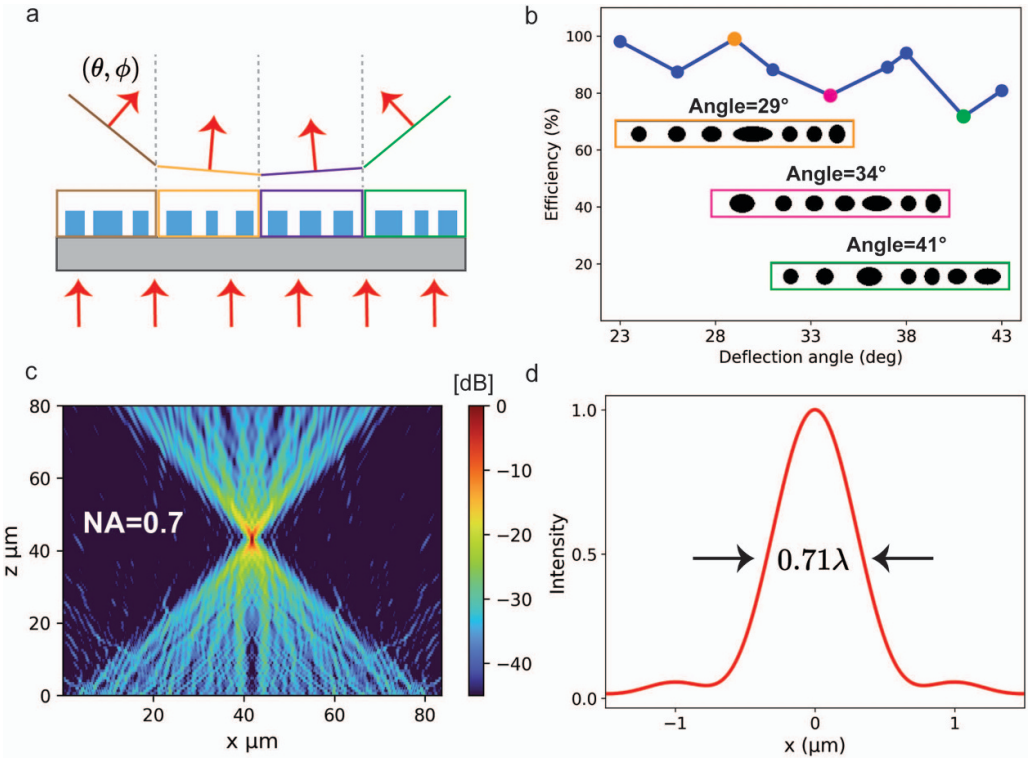

Figure 4. Large-area, reparameterized freeform metasurfaces. (a) Schematic of the design concept: the full wavefront profile is divided into a series of wavelength-scale, linear scatterers and each scatterer is designed to scatter light with a specific angle (θ) and phase (ϕ). (b) The absolute deflection efficiency of super-pixels for a range of angles. (c) Full-wave simulation of the axial intensity distribution of a 0.7 NA metalens on a dB scale. (d) One-dimensional horizontal cut of intensity at the focal plane.

the field intensity at the focal plane (figure 4(d)) shows that the full wave half maximum is close to diffraction-limited performance.

In summary, we present a facile design framework for freeform metasurfaces comprising nearly uniform nanopost elements. Despite the constrained design space, our approach incorporates nonlocal interactions between neighboring elements without approximation that enable highly efficient beam scattering. We further apply our concept to the design of a large-area, high-numerical-aperture metalens that supports high-efficiency, diffraction-limited focusing. These design concepts present more straightforward experimental avenues for the reliable manufacturing of metasurfaces, which remains challenging for devices made using freeform design algorithms. We anticipate further research directions that incorporate element shapes beyond ellipses and that accelerate

the optimization process with high-speed electromagnetic solvers [47–49].

Data availability statement

All data that support the findings of this study are included within the article (and any supplementary files).

Acknowledgments

This work was supported by the Department of Energy and Lawrence Livermore National Lab Contract No. DE-AC52-07NA27344, the Office of Naval Research under Award Number N00014-20-1-2105, and the National Science Foundation under Award 2103301.

Conflict of interest

The authors declare no conflict of interest.

ORCID iDs

You Zhou https://orcid.org/0000-0002-5810-2347
Yixuan Shao https://orcid.org/0009-0009-6130-2831

References

[1] Khorasaninejad M, Chen W T, Devlin R C, Oh J, Zhu A Y and Capasso F 2016 Metalenses at visible wavelengths: diffraction-limited focusing and subwavelength resolution imaging *Science* **352** 1190–4
[2] Chen W T, Zhu A Y, Sanjeev V, Khorasaninejad M, Shi Z, Lee E and Capasso F 2018 A broadband achromatic metalens for focusing and imaging in the visible *Nat. Nanotechnol.* **13** 220–6
[3] Zhou Y, Kravchenko I I, Wang H, Nolen J R, Gu G and Valentine J 2018 Multilayer noninteracting dielectric metasurfaces for multiwavelength metaoptics *Nano Lett.* **18** 7529–37
[4] Zheng H, Zhou Y, Ugwu C F, Du A, Kravchenko I I and Valentine J G 2021 Large-scale metasurfaces based on grayscale nanosphere lithography *ACS Photonics* **8** 1824–31
[5] Wang L, Kruk S, Tang H, Li T, Kravchenko I, Neshev D N and Kivshar Y S 2016 Grayscale transparent metasurface holograms *Optica* **3** 1504
[6] Zheng G, Mühlenbernd H, Kenney M, Li G, Zentgraf T and Zhang S 2015 Metasurface holograms reaching 80% efficiency *Nat. Nanotechnol.* **10** 308–12
[7] Arbabi E, Kamali S M, Arbabi A and Faraon A 2018 Full-stokes imaging polarimetry using dielectric metasurfaces *ACS Photonics* **5** 3132–40
[8] Rubin N A, D'Aversa G, Chevalier P, Shi Z, Chen W T and Capasso F 2019 Matrix Fourier optics enables a compact full-Stokes polarization camera *Science* **364** eaax1839
[9] Slovick B A, Zhou Y, Yu Z G, Kravchenko I I, Briggs D P, Moitra P, Krishnamurthy S and Valentine J 2017 Metasurface polarization splitter *Phil. Trans. R. Soc.* A **375** 20160072
[10] Wang E W, Phan T, Yu S-J, Dhuey S and Fan J A 2022 Dynamic circular birefringence response with fractured geometric phase metasurface systems *Proc. Natl Acad. Sci.* **119** e2122085119
[11] Wang E W, Yu S, Phan T, Dhuey S and Fan J A 2023 Arbitrary achromatic polarization control with reconfigurable metasurface systems *Laser Photon. Rev.* **17** 2200926
[12] Zhou Y, Kravchenko I I, Wang H, Zheng H, Gu G and Valentine J 2019 Multifunctional metaoptics based on bilayer metasurfaces *Light Sci. Appl.* **8** 1–9
[13] Lin D, Holsteen A L, Maguid E, Wetzstein G, Kik P G, Hasman E and Brongersma M L 2016 Photonic multitasking interleaved Si nanoantenna phased array *Nano Lett.* **16** 7671–6
[14] Wang X, Wang H, Wang J, Liu X, Hao H, Tan Y S, Zhang Y, Zhang H, Ding X and Zhao W 2023 Single-shot isotropic differential interference contrast microscopy *Nat. Commun.* **14** 2063
[15] Chen J, Yu F, Liu X, Bao Y, Chen R, Zhao Z, Wang J, Wang X, Liu W and Shi Y 2023 Polychromatic full-polarization control in mid-infrared light *Light Sci. Appl.* **12** 105
[16] Zhou Y and Fan J A 2023 Polychromatic metasurfaces for complete control of phase and polarization in the mid-infrared *Light Sci. Appl.* **12** 249
[17] Overvig A and Alù A 2022 Diffractive nonlocal metasurfaces *Laser Photon. Rev.* **16** 2100633
[18] Zhou Y, Guo S, Overvig A C and Alù A 2023 Multiresonant nonlocal metasurfaces *Nano Lett.* **23** 6768–75
[19] Zhou Y, Zheng H, Kravchenko I I and Valentine J 2020 Flat optics for image differentiation *Nat. Photon.* **14** 316–23
[20] Overvig A and Alù A 2021 Wavefront-selective Fano resonant metasurfaces *Adv. Photon.* **3** 1–11
[21] Ji A, Song J-H, Li Q, Xu F, Tsai C-T, Tiberio R C, Cui B, Lalanne P, Kik P G and Miller D A B 2022 Quantitative phase contrast imaging with a nonlocal angle-selective metasurface *Nat. Commun.* **13** 7848
[22] Park J S, Zhang S, She A, Chen W T, Lin P, Yousef K M A, Cheng J X and Capasso F 2019 All-glass, large metalens at visible wavelength using deep-ultraviolet projection lithography *Nano Lett.* **19** 8673–82
[23] Khorasaninejad M, Zhu A Y, Roques-Carmes C, Chen W T, Oh J, Mishra I, Devlin R C and Capasso F 2016 Polarization-insensitive metalenses at visible wavelengths *Nano Lett.* **16** 7229–34
[24] Arbabi A, Horie Y, Ball A J, Bagheri M and Faraon A 2015 Subwavelength-thick lenses with high numerical apertures and large efficiency based on high-contrast transmitarrays *Nat. Commun.* **6** 7069
[25] Lalau-Keraly C M, Bhargava S, Miller O D and Yablonovitch E 2013 Adjoint shape optimization applied to electromagnetic design *Opt. Express* **21** 21693
[26] Molesky S, Lin Z, Piggott A Y, Jin W, Vucković J and Rodriguez A W 2018 Inverse design in nanophotonics *Nat. Photon.* **12** 659–70
[27] Chen M *et al* 2024 Validation and characterization of algorithms and software for photonics inverse design *J. Opt. Soc. Am.* B **41** A161
[28] Jiang J and Fan J A 2019 Global optimization of dielectric metasurfaces using a physics-driven neural network *Nano Lett.* **19** 5366–72
[29] Sell D, Yang J, Doshay S, Yang R and Fan J A 2017 Large-angle, multifunctional metagratings based on freeform multimode geometries *Nano Lett.* **17** 3752–7
[30] Sell D, Yang J, Doshay S and Fan J A 2017 Periodic dielectric metasurfaces with high-efficiency, multiwavelength functionalities *Adv. Opt. Mater.* **5** 1–7
[31] Lin Z, Groever B, Capasso F, Rodriguez A W and Lončar M 2018 Topology-optimized multilayered metaoptics *Phys. Rev. Appl.* **9** 044030

[32] Mansouree M, McClung A, Samudrala S and Arbabi A 2021 Large-scale parametrized metasurface design using adjoint optimization *ACS Photonics* **8** 455–63
[33] Phan T, Sell D, Wang E W, Doshay S, Edee K, Yang J and Fan J A 2019 High-efficiency, large-area, topology-optimized metasurfaces *Light Sci. Appl.* **8** 48
[34] Roberts G, Ballew C, Zheng T, Garcia J C, Camayd-Muñoz S, Hon P W C and Faraon A 2023 3D-patterned inverse-designed mid-infrared metaoptics *Nat. Commun.* **14** 2768
[35] Wang E W, Sell D, Phan T and Fan J A 2019 Robust design of topology-optimized metasurfaces *Opt. Mater. Express* **9** 469–82
[36] Qian X, Yuan M, Khoram E and Yu Z 2020 Controlling the minimal feature sizes in adjoint optimization of nanophotonic devices using b-spline surfaces *Opt. Express* **28** 7060–9
[37] Shen B, Wang P, Polson R and Menon R 2015 An integrated-nanophotonics polarization beamsplitter with $2.4\times$ 2.4 μm^2 footprint *Nat. Photon.* **9** 378–82
[38] Hammond A M, Oskooi A, Johnson S G and Ralph S E 2021 Photonic topology optimization with semiconductor-foundry design-rule constraints *Opt. Express* **29** 23916
[39] Mansouree M, Kwon H, Arbabi E, McClung A, Faraon A and Arbabi A 2020 Multifunctional 2.5 D metastructures enabled by adjoint optimization *Optica* **7** 77–84
[40] Jensen J S and Sigmund O 2005 Topology optimization of photonic crystal structures: a high-bandwidth low-loss T-junction waveguide *J. Opt. Soc. Am.* B **22** 1191–8
[41] Zhou M, Lazarov B S, Wang F and Sigmund O 2015 Minimum length scale in topology optimization by geometric constraints *Comput. Methods Appl. Mech. Eng.* **293** 266–82
[42] Vercruysse D, Sapra N V, Su L, Trivedi R and Vučković J 2019 Analytical level set fabrication constraints for inverse design *Sci. Rep.* **9** 8999
[43] Gershnabel E, Chen M, Mao C, Wang E W, Lalanne P and Fan J A 2022 Reparameterization approach to gradient-based inverse design of three-dimensional nanophotonic devices *ACS Photonics* **10** 815–23
[44] Oskooi A F, Roundy D, Ibanescu M, Bermel P, Joannopoulos J D and Johnson S G 2010 MEEP: a flexible free-software package for electromagnetic simulations by the FDTD method *Comput. Phys. Commun.* **181** 687–702
[45] Ra'di Y, Sounas D L and Alu A 2017 Meta-gratings: beyond the limits of graded metasurfaces for wavefront control *Phys. Rev. Lett.* **119** 1–6
[46] Zhou Y, Mao C, Gershnabel E, Chen M and Fan J A 2024 Large-area, high-numerical-aperture, freeform metasurfaces *Laser Photon. Rev.* 2300988
[47] Chen M, Lupoiu R, Mao C, Huang D-H, Jiang J, Lalanne P and Fan J A 2022 High speed simulation and freeform optimization of nanophotonic devices with physics-augmented deep learning *ACS Photonics* **9** 3110–23
[48] Augenstein Y, Repän T and Rockstuhl C 2023 Neural operator-based surrogate solver for free-form electromagnetic inverse design *ACS Photonics* **10** 1547–57
[49] Li Z, Pestourie R, Park J-S, Huang Y-W, Johnson S G and Capasso F 2022 Inverse design enables large-scale high-performance meta-optics reshaping virtual reality *Nat. Commun.* **13** 2409